AGU PUBLICATIONS

JGR

Journal of Geophysical Research: Oceans

RESEARCH ARTICLE

10.1002/2015JC011057

Climate controls multidecadal variability in U. S. extreme sea level records

Thomas Wahl[1] and Don P. Chambers[1]

[1]College of Marine Science, University of South Florida, St. Petersburg, Florida, USA

Key Points:
- Four climate indices explain much of the decadal variations in U.S. extreme sea levels
- Tailored indices and wind stress curl allow improved predictions
- The predictions can be used as covariates for extreme value analysis

Supporting Information:
- Supporting Information S1

Correspondence to:
T. Wahl,
thomaswahl@mail.usf.edu

Citation:
Wahl, T., and D. P. Chambers (2016), Climate controls multidecadal variability in U. S. extreme sea level records, *J. Geophys. Res. Oceans*, *121*, 1274–1290, doi:10.1002/2015JC011057.

Received 16 JUN 2015
Accepted 20 JAN 2016
Accepted article online 25 JAN 2016
Published online 12 FEB 2016

Abstract We investigate the links between multidecadal changes in extreme sea levels (expressed as 100 year return water levels (RWLs)) along the United States coastline and large-scale climate variability. We develop different sets of simple and multiple linear regression models using both traditional climate indices and tailored indices based on nearby atmospheric/oceanic variables (winds, pressure, sea surface temperature) as independent predictors. The models, after being tested for spatial and temporal stability, are capable of explaining large fractions of the observed variability, up to 96% at individual sites and more than 80% on average across the region. Using the model predictions as covariates in a quasi nonstationary extreme value analysis also significantly reduces the range of change in the 100 year RWLs over time, turning a nonstationary process into a stationary one. This suggests that the models—when used with regional and global climate model output of the predictors—will also be capable of projecting future RWL changes. Such information is highly relevant for decision makers in the climate adaptation context in addition to projections of long-term sea level rise.

1. Introduction

Most climatic variables exhibit considerable fluctuations at time scales ranging from months (e.g., seasonality) to several decades, which are superimposed onto the underlying long-term trends. In sea level research, efforts to understand the driving mechanisms of the observed variability inherent to the system have mostly been directed toward mean sea level (MSL), as one of the most important indicators for climatic change [e.g., *Church et al*., 2013]. Changes in extreme sea levels can, however, be more important than MSL changes for coastal regions, but have had less attention in the past. A rigorous assessment with the main objective of identifying the (design-) relevant variations in extreme sea levels along the U.S. coastline unrelated to MSL changes, and associated 100 year return water levels (RWLs), was conducted by *Wahl and Chambers* [2015] (hereafter referred to as W15).

The key findings of that study are summarized in Figure 1, showing: (1) the locations of the 20 tide gauges that were used in W15; for all sites hourly water level observations are available for the common period 1929–2013; (2) six regions which have been identified to exhibit coherent multidecadal variability; (3) the relevant season (here we split the year into halves) when storm surges tend to be larger along a particular coastline stretch; tropical cyclones dominate the storm surge climate in summer (S) (May–November) and extratropical cyclones in winter (W) (December–April); (4) the tide gauges which have been selected as being representative for each of the six regions (and the relevant seasons); and (5) the temporal variations in 100 year RWLs. The latter were obtained with a quasi nonstationary extreme value analysis based on annual maxima and a 37 year (i.e., twice the nodal cycle) running window approach; the changes through time are compared to the 95% confidence levels derived from the stationary analysis. The results shown in Figure 1 were cross validated with neighboring sites and by applying a range of different sampling and inference techniques.

In total, eight time series were identified which explain a major portion of the relevant multidecadal variability in extreme sea levels along the U.S. coast unrelated to MSL change. The fluctuations in 100 year RWLs range from a few centimeters to several decimeters and deviate significantly from the stationary assumption in all eight cases. These results suggest that accounting for future decadal variability is crucial for coastal adaptation planning, in order to provide sufficiently high safety standards throughout the expected lifetimes of new and existent infrastructure, or when adapting/restoring natural protection measures such

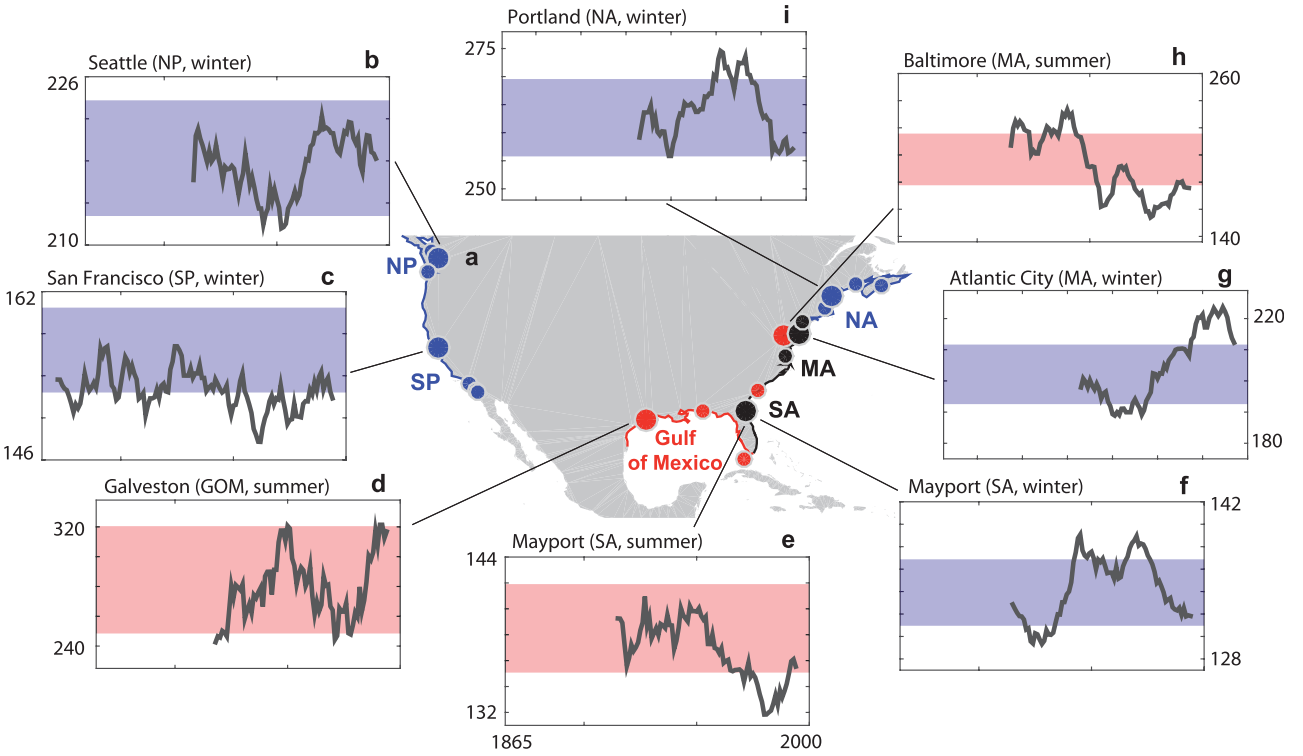

Figure 1. (a) Location of the 20 tide gauges used in W15 (circles); regions with coherent multidecadal extreme sea level variability (i.e., North Pacific, NP; South Pacific, SP; Gulf of Mexico, GOM; South Atlantic, SA; Mid Atlantic, MA; and North Atlantic NA); the relevant season(s) for each region (red: summer; blue: winter; gray: both); and tide gauges assumed to be representative of a respective region (larger circles). (b–i) Temporal changes (in centimeters) in 100 year RWLs derived with the quasi nonstationary extreme value analysis applied in W15 compared to the results obtained with a stationary analysis (shaded bars; red: summer; blue: winter).

as dunes or berms. After identifying the relevant variations, the next important step to accomplish the aforementioned long-term objective of projecting future changes lies in exploring and understanding the driving mechanisms.

Several studies have investigated the links between extreme sea levels along different parts of the U.S. coastline and large-scale climate variability. It is known, for example, that indices resembling (or being influenced by) the El-Niño Southern Oscillation (ENSO) phenomenon and activity (e.g., Southern Oscillation Index (SOI), Pacific Decadal Oscillation (PDO), Pacific-North America pattern, Multivariate ENSO Index, North Pacific Index (NPI), Niño 3.4 index) are linked to the storm surge climate along the U.S. west coast [e.g., *Bromirski et al*., 2003; *Cayan et al*., 2008; *Komar et al*., 2011; *Méndez et al*., 2007; *Serafin and Ruggiero*, 2014] (i.e., the South Pacific and North Pacific regions in this study). ENSO has also been shown to be related to the tropical cyclone activity (in combination with the NAO determining the tracks) in the North Atlantic and Gulf of Mexico [e.g., *Elsner*, 2003; *Kennedy et al*., 2007]. This in turn affects the storm surge climate, especially during the tropical cyclone season (May–October) in the Gulf of Mexico and South Atlantic regions (as defined in Figure 1a), as well as the extratropical cyclone activity (mainly from December to April) along the U.S. east coast [e.g., *Sweet and Zervas*, 2011] (Mid Atlantic and North Atlantic regions in this study). *Park et al*. [2010a,b] also highlighted a strong connection between extreme sea levels observed around Florida and the Atlantic Multidecadal Oscillation (AMO); *Talke et al*. [2014] identified a close link between storm surges observed at the Battery tide gauge in New York City and the North Atlantic Oscillation (NAO).

In many of those studies, the focus was on exploring the relationship between large-scale climate and interannual extreme sea level variability, whereas different mechanisms may act on longer time scales driving the observed multidecadal changes reported in W15 for the U.S. coast, and by *Marcos et al*. [2015] at the global scale. Furthermore, each of the aforementioned studies used a different definition of extreme sea level events—e.g., different thresholds of storm surge heights (with tide included or removed), storm (surge) counts, storm surge intensity, or RWLs—and the results are therefore not directly comparable.

Table 1. Summary of the Climate Indices Used in the Present Study

Index	Period Covered	Description	Selected Reference
Atlantic multidecadal oscillation (AMO)	1856–2013	Area-averaged SST (Kaplan) in the Atlantic north of 0°	*Enfield et al.* [2001]
Arctic oscillation (AO)	1871–2011	Projection of 1000 mb height anomalies (from 20CR) onto first EOF poleward of 20°N	*Thompson and Wallace* [1998]
North Atlantic oscillation (NAO)	1865–2013	Difference of normalized SLP between Lisbon and Stykkisholmur/Reykjavik	*Hurrell* [1995]
Niño1 + 2 (N12)	1870–2013	Area-averaged SST (HadISST1) from 0° to 10°S and 90° to 80°W	*Rayner et al.* [2003]
Niño3 (N3)	1870–2013	Area-averaged SST (HadISST1) from 5°S to 5°N and 150° to 90°W	*Rayner et al.* [2003]
North Pacific index (NPI)	1899–2013	Area-weighted SLP 30° to 65°N, 160°E to 140°W.	*Trenberth and Hurrell* [1994]
Pacific decadal oscillation (PDO)	1900–2013	Leading EOF of monthly SST anomalies over the North Pacific (poleward of 20°N); global average SST anomalies are removed	*Mantua et al.* [1997]
Southern oscillation index (SOI)	1866–2013	Normalized pressure difference between Tahiti and Darwin	*Ropelewski and Jones* [1987]

Here, we use the results from W15 and apply a consistent approach to explore the connection between multidecadal RWL variations along the U.S. coastline and large-scale climate in the region. Simple and multiple linear regression models are developed and evaluated in terms of their capability of reconstructing the observed RWL changes. As predictors we use various climate indices that have been shown in earlier studies to affect the climate over the North American continent and its coastal waters. However, originally these indices were not developed or defined with the specific aim of explaining multidecadal RWL variability. The PDO, as an example, was first introduced by *Mantua et al*. [1997] while investigating climate impacts on salmon production in the North Pacific (whereas they also already noted impacts on streamflow and coastal waters). Therefore, in addition, we develop new indices—which are then also used as alternative predictors in the regression models—from gridded sea level pressure (SLP), sea surface temperature (SST), and wind stress curl. Those indices are specifically tailored toward the objective of this study, i.e., explaining multidecadal RWL changes along the U.S. coast. Similar approaches were used for example by *Thompson et al*. [2013] and *Dangendorf et al*. [2014] to investigate storminess variability along the U.S. east coast and in the North Sea, respectively, and by *Grinsted et al*. [2013] to project the Atlantic hurricane surge threat.

The data sets used for the analyses are described in section 2, the model development is summarized in section 3, results from evaluating the different models are presented in section 4, and a summary of the key findings and conclusions are provided in section 5.

2. Data

The sources of the tide gauge data that were used to derive the time series of changes in RWLs are described in detail in W15. For the simple regression analysis (see Methods and Results), we consider the eight climate indices listed in Table 1. The table provides information about the periods that are covered by the different indices, a brief description of how they are derived, and selected references; in addition to the ones listed here we also tested the Pacific-North America pattern and Multivariate ENSO Index, but found that they did not add additional information to the study. The time series of the climate indices are freely accessible through different websites (see Acknowledgements).

Tailored indices are derived from NOAA's Extended Reconstructed SST v3b (available on a 2° × 2° grid and covering the period 1854–2013), and SLP and wind stress curl (calculated from zonal and meridional winds) are obtained from the 20th Century Reanalysis Project [*Compo et al*., 2011] (available on a 2° × 2° grid and covering the period 1871–2012).

Both the traditional and tailored indices used in the study are calculated separately for the tropical (May–November) and extratropical (December–April) cyclone seasons. They are also low-pass filtered with a 37

year moving average in order to allow direct comparison to the RWL time series derived with the extreme value analysis in W15 (which also uses a 37 year running window equaling twice the length of the nodal cycle; Figures 1b–1i).

3. Methods

3.1. Simple Linear Regression With Climate Indices

We start by building two sets of simple linear regression models. For the first one, we identify the climate indices showing the strongest correlations with the time series of location and scale parameters derived with the quasi nonstationary extreme value analysis in W15 (see Figure 10 in their paper). The latter were then used along with the stationary shape parameter of the Generalized Extreme Value distribution to obtain the 100 year RWL time series depicted in Figures 1b–1i. Hence, regression models are also first derived for the location and scale parameters and both are predicted separately before they are used together with the shape parameter to reconstruct the RWL time series; this model is denoted SLRM0. For the second set of models, we directly correlate the low-pass filtered climate indices with the RWL time series and use the one with the strongest correlation to reconstruct the observed temporal RWL changes; this model setup is denoted SLRM1.

Note that we generally use the climate index with the strongest correlation in the models; however, if two or more indices exhibit strong correlation with the RWL time series (which also suggests considerable cross correlation between the different climate indices), we select the one that seems more plausible to affect extreme sea levels at a particular site. For example, if ENSO and NAO are both significantly correlated with a tide gauge on the west coast of United States, we select ENSO as the predictor as it is more likely from a process-based understanding to affect west coast extreme sea levels than the NAO.

Significance of correlation is assessed here in two different ways. When we compare results from the extreme value analysis with smoothed climate indices we use a resampling approach, i.e., we shuffle the seasonal maxima values used in W15 (which are approximately independent and identically distributed) and repeat the quasi nonstationary extreme value analysis to obtain 1000 surrogate time series of RWLs, as well as location and scale parameters for the sites and seasons shown in Figure 1. Then we correlate each one with the smoothed climate indices and obtain the 5% and 95% levels (equals the 90% confidence level); when the actual correlation falls outside this region, it is deemed significant. We also quantify the cross correlation between the smoothed climate indices. In this case, we have to follow a different approach for assessing significance since the underlying data already exhibits autocorrelation before the smoothing is applied. Thus, we use a *t*-test where we reduce the number of degrees of freedom according to the window length that is used for the low-pass filtering (here 37 years); if there are for example 148 overlapping data points we use only 4 degrees of freedom in the *t*-test. This approach is conservative because it does not account for the weakening autocorrelation when moving forward in time; when two smoothed data points are for example 36 years apart they only share one common (raw) value and are therefore virtually independent whereas we assume that they are fully dependent. We account for this by assessing significance at the relatively low one-sigma level.

3.2. Simple and Multiple Linear Regression With Tailored Indices

In order to develop tailored indices, which are expected to allow a better and physically more consistent reconstruction of observed RWL changes, we first analyze the spatial patterns derived from the pointwise correlation between the low-pass filtered climate indices and the gridded variables they were derived from, i.e., either SST or SLP (the time series of all grid points are also low-pass filtered with a 37 year moving average). This analysis step reveals the location of the centers of action (COAs) of the climate indices in the summer and winter half years after they have been low-pass filtered. These are the regions we focus on in the next step when performing the pointwise correlation between the RWL time series and low-pass filtered gridded SST or SLP. For each site, we develop two sets of tailored indices (referred to as primary and secondary indices), one derived from SST the other from SLP. The decision of which one is considered the primary index is guided by the results from the correlation analysis with "traditional climate indices." For example, if at a particular site a strong relationship between RWL changes and the PDO was identified the primary index is based on the pointwise correlation between the RWL time series and the low-pass filtered gridded SST (for the relevant season); the secondary index comes from SLP. If the NAO (or one of the other

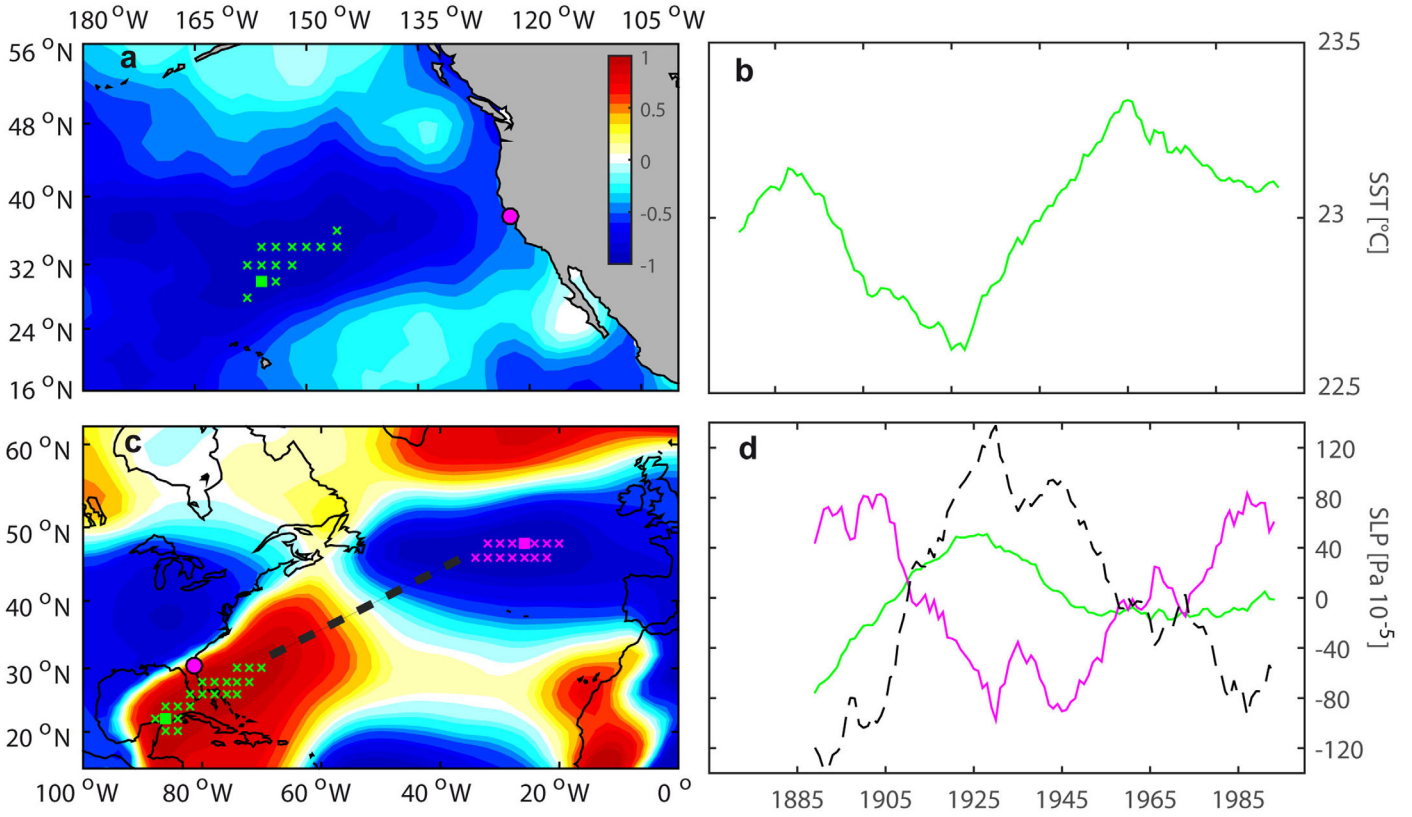

Figure 2. Procedure to derive tailored indices from SST (a–b; San Francisco, winter) and SLP (c–d; Mayport, summer). (a, c) Filled squares mark the grid points with the highest (lowest) correlation; crosses show regions with correlation within 5% of the maxima (minima) and magenta filled circles denote the tide gauge location. (b) Tailored index for San Francisco derived by averaging the SST from grid points marked in Figure 2a. (d) Average SLP from grid points with the lowest (magenta) and highest (green) correlation marked in Figure 2c and the tailored index (black-dashed) for Mayport derived by subtracting the two.

pressure-based indices) showed the strongest correlation, we use SLP for the primary index and SST for the secondary index. The spatial stability of the regions with high/low values derived from the pointwise correlation between RWLs and SST/SLP is tested by repeating the same analysis but using only the first and second halves of the available time series. The regions with persistent strong correlation where a physical relationship to RWL variations at a particular site is also plausible are then used to build the tailored indices.

Once this is done, we search for the grid points with the strongest correlation within the COAs and all grid points exhibiting correlations within 5% of the maxima/minima. In cases where we use SST, we find only one COA (Figure 2a) and the tailored indices are derived by averaging the low-pass filtered time series from the grid points fulfilling the aforementioned criteria (Figure 2b). When we use SLP, we often find a dipole comprised of two COAs (one with positive correlation, one with negative correlation) (Figure 2b); in these cases, the tailored indices represent the pressure gradients between the two COAs derived from averaged SLP time series sharing the strongest positive and negative correlation with RWL changes (Figure 2d).

The primary tailored indices are used to develop a third set of simple regression models (denoted SLRM2), before multiple regression models (denoted as MLRM1) are derived with both the primary and secondary tailored indices as independent predictors. The latter is to acknowledge the dynamic coupling between SST and SLP and their respective effects on storminess, with SST being closer related to cyclogenesis and SLP to storm tracks [e.g., *Elsner*, 2003].

In general, the occurrence of extreme sea level events requires strong winds blowing onshore pushing water toward the coastline. To account for this, we develop a final set of models (denoted MLRM2) using multiple linear regression with both sets of tailored indices and wind stress curl as predictors. For wind stress curl, we use the low-pass filtered (37 year moving average) time series of the grid point with the strongest correlation within 10° around a particular tide gauge location.

In all multiple regression models used for the study, we include terms to account for interaction effects between the different predictors; i.e., the contribution of one predictor to the dependent variable may be stronger or weaker conditional on the state of one of the other predictors [e.g., *Jaccard et al*., 1990]. Hence, the relationship between RWL at a tide gauge at time t and the independent variables, $x_{t1}, x_{t2}, \ldots, x_{tp}$, is given by

$$RWL_t = \mathbf{x}_t^{\mathrm{T}}\beta + u_t, t = 1, 2, \ldots, n \quad (1)$$

where $^{\mathrm{T}}$ is the transpose, $\mathbf{x}_t = (1, x_{t1} = t, \ldots, x_{tp}, x_{t1}\ x_{t2}, \ldots, x_{tp-1}\ x_{tp})^{\mathrm{T}}$, $\beta = (\beta_0, \beta_1, \ldots, \beta_p)^{\mathrm{T}}$ is a $(p+1)$-dimensional vector containing the regression coefficients, and u_t is an error term.

4. Results

4.1. Simple Regression With Traditional Climate Indices

The correlation analysis in Figure 3 shows that, with a few exceptions (e.g., San Francisco and Galveston), there is generally at least one climate index exhibiting significant correlation with the RWL time series and the strongest absolute correlation is at least 0.6 at all sites. In many cases, more than one climate index shows strong (or even significant) correlation with the RWL time series suggesting considerable cross correlation of the climate indices with each other (Figures 3d and 3e). Especially in winter, when the signals of some of the indices are stronger, the correlation between them is large and often significant. For the purpose of the present study, this suggests that they also share and contribute the same information to the regression models.

We do not use the climate index with the strongest correlation when it is physically more plausible that one of the others (with similar correlation) has a more direct effect on extreme sea levels at a particular site. This may be the case when teleconnection patterns are intimately linked at multidecadal time scales (as suggested from Figures 3d and 3e). However, given the relatively small number of degrees of freedom in the analysis, we can also not rule out that high correlations occur simply by chance, which would imply that the resulting regression models are not generalizing the problem very well. Therefore, the more detailed analysis using the SST and SLP fields and testing the robustness of spatial correlation patterns (see section 4.2) is important.

Here, for the SLRM0 models (i.e., location and scale parameters are predicted separately and then used to obtain RWLs), we use AMO as predictor for the location parameter at Mayport (S) although NPI has a slightly stronger correlation, but its footprint is mainly in the Pacific. The AMO on the other hand has been found to be related to the size of the Atlantic warm pool, which in turn affects the Atlantic hurricane activity [*Park et al*., 2010a,b and references therein] and hence the storm surge climate in the southeastern U.S. and Gulf of Mexico during the summer months; note that AMO is also selected at Galveston (S). Furthermore, we select the NAO as predictor in winter for the location parameter at Mayport (instead of PDO), the scale parameter at Portland (instead of NPI), and for RWL (in the SLRM1 models) at the same two sites instead of the PDO. Both tide gauges are located at the east coast and therefore it seems more plausible that extreme sea levels are affected by the NAO [e.g., *Bernhardt and DeGaetano*, 2012]—especially in winter when the signal is stronger—than by the PDO, which is derived from SST anomalies in the Pacific. We use AMO as a predictor for Seattle—even if the tide gauge is located at the northwest coast—as it is the only index showing significant correlation in all three cases (location and scale parameters, and RWLs).

The SLRM0 models explain between 33% (San Francisco) and 81% (Atlantic City) of the variability of the 100 year RWL time series (57% on average) (Figure 4). The explained variance with the SLRM1 models ranges from 34% (Galveston) to 81% (Atlantic City) and the average is slightly higher (59%) (Figure 4). In most cases, the results from both models are similar (or even identical) and the RWL time series derived from observations in W15 are within the 95% confidence bounds obtained from the SLRM1 predictions. None of the two models leads to significantly better results than the other. Therefore, in order to keep the complexity at a minimum, we prefer the direct approach and the following models SLRM2, MLRM1, and MLRM2 are developed to directly predict RWL variations instead of the location and scale parameters separately. The model results also highlight that only four of the climate indices (AMO, AO, NAO, and PDO) are required to explain a major fraction of the observed multi-decadal variability along the U.S. coastline.

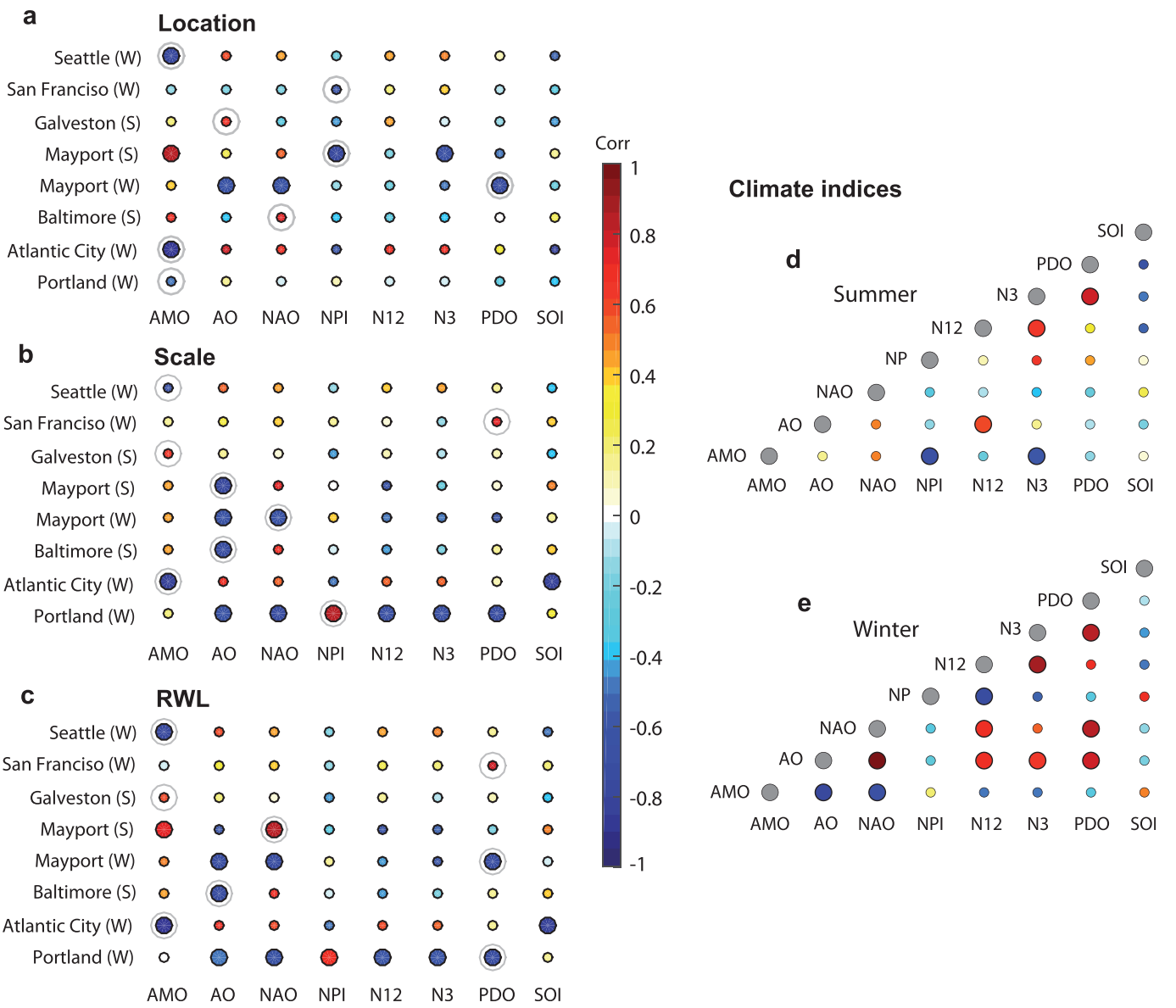

Figure 3. (a–c) Correlation between low-pass filtered climate indices and (a) the location parameter, (b) scale parameter, and (c) 100 year RWL time series derived in W15 at representative sites and for the relevant seasons; time series pairs with the highest correlations (for each climate index) are highlighted by circle frames. (d, e) Cross correlation between the low-pass filtered climate indices used in the present study for summer (d) and winter (e) half years. Larger circles denote significant correlation (at the one-sigma level).

4.2. Development of Tailored Indices

The results from the pointwise correlation between low-pass filtered SST/SLP and the four climate indices that explain most of the RWL changes are shown in Figure 5; results for the other four indices are shown in supporting information Figure S1.

The COA of the smoothed AMO is confined to the North Atlantic, with the strongest correlation in the region between Iceland and the British Isles. However, there is also a region of strong correlation in the northeastern Pacific that is likely the source of relationship between Seattle RWLs and the AMO shown in Figure 4. The AO is marked by low correlation with SLP at higher latitudes and high correlation at lower latitudes; it also shows similarity with the NAO, as expected from the results presented in Figures 3d and 3e. The location and size of the two COAs representing the NAO are different in summer (in the North Atlantic between the U.S. northeast coast and Europe and over the Gulf of Mexico) compared to winter, where both COAs are wider and shifted northward (in addition to changing the sign). For the PDO, we find strong negative correlation with SST in the northern Pacific, which extends west all the way to Japan, and positive

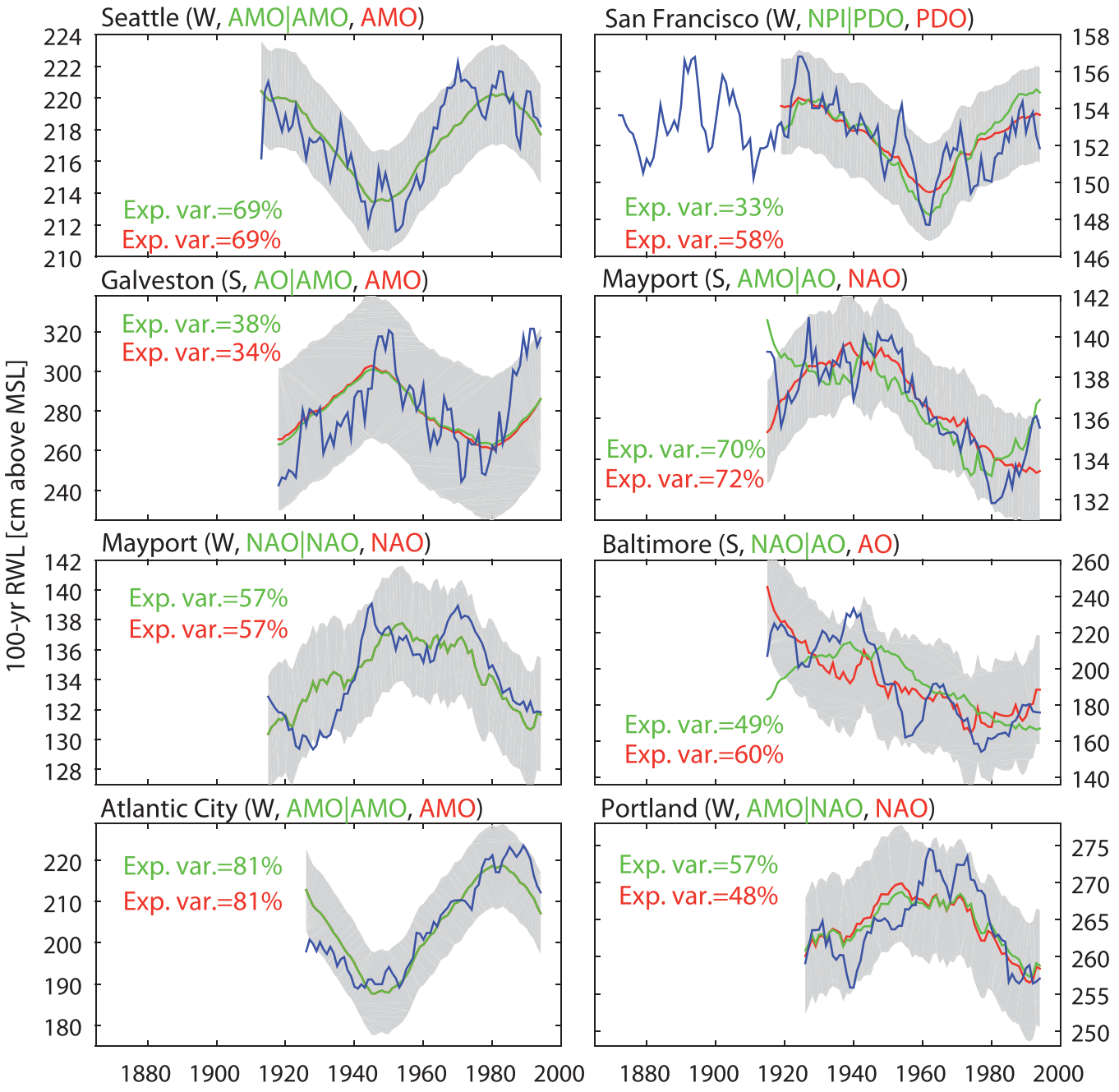

Figure 4. Observed (blue) and predicted RWL changes with the SLRM0 (green) and SLRM1 (red) models; captions denote the indices that are used as predictors and numbers indicate the amount of the explained variance. Shaded gray areas represent 95% confidence levels from the SLRM1 predictions.

correlation in the Niño 3.4 region in the tropical pacific and Niño 1 + 2 region off the northwest coast of South America. The other four indices (supporting information Figure S1) also resemble the known spatial features, with the NPI showing strong correlation with SLP in the northeast Pacific, N3 and N12 being closely related to SST in the tropical Pacific, and SOI showing a pressure dipole between the western and eastern tropical Pacific.

Next, we perform the pointwise correlation between the RWL time series and low-pass filtered SST/SLP; first for the entire record lengths, and then for the first and second halves to test the spatial stability of the results. Correlation maps for the variables (SST or SLP) that were selected to be used for the primary tailored indices are shown in Figure 6; those for the other variable at each site (used for the secondary indices) are

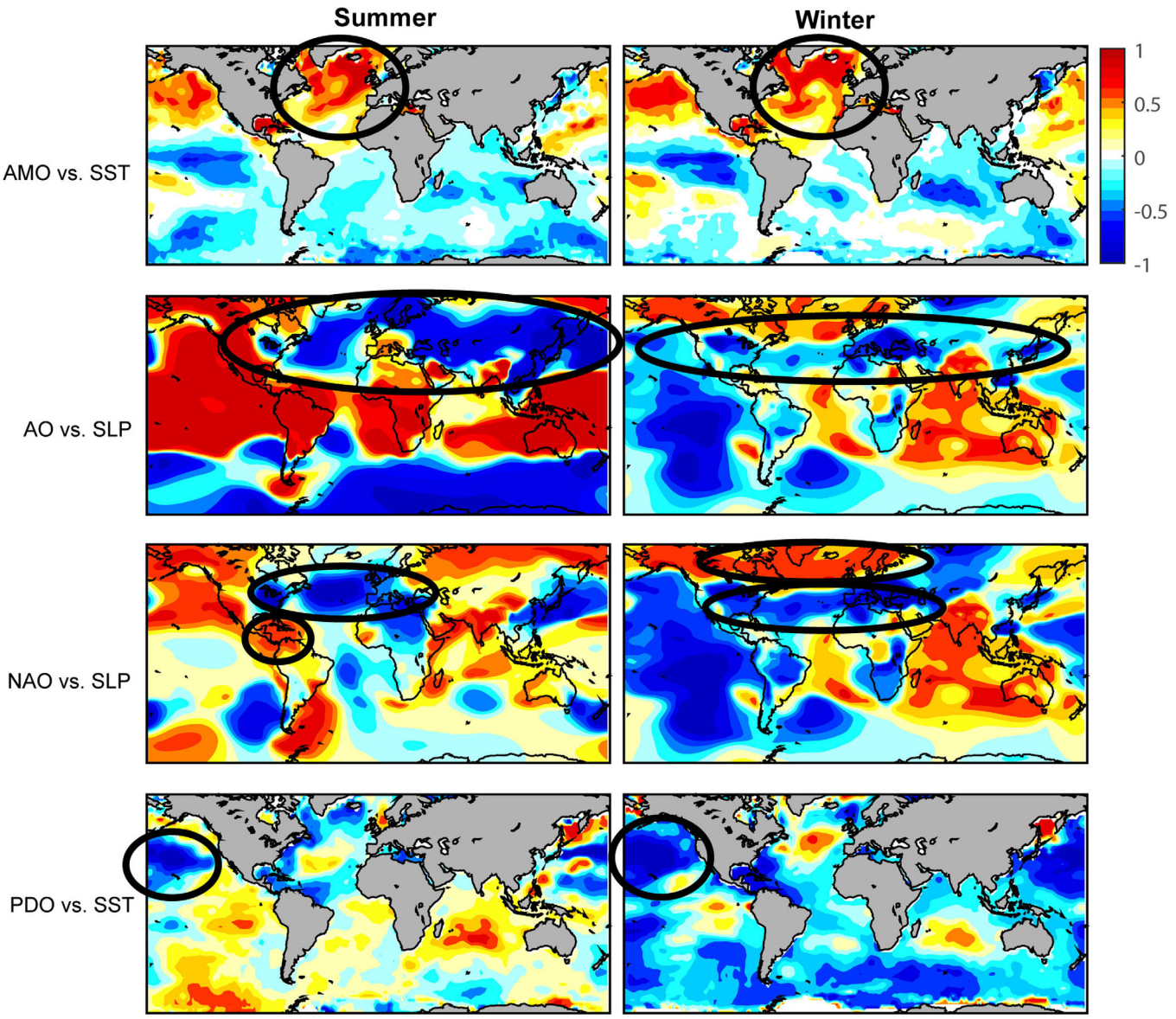

Figure 5. Pointwise correlation between four low-pass filtered climate indices and SLP or SST for summer (left) and winter (right); COAs are highlighted.

shown in supplementary information Figure S2. For Seattle (W), we found a strong relationship between the winter RWL time series and the AMO in the previous analysis step; this is confirmed here by the persistent strong negative correlation between RWL and SST in the North Atlantic around Iceland. We also find another region off the U.S. northwest coast where the correlation is almost as strong (note that the same region stands out in Figure 5). In this case, it seems more likely that the SST in this region affects extreme sea levels at Seattle than the SST in the North Atlantic, although connections between the AMO and North Pacific climate variability have been suggested, but with a time lag of several years [*Zhang and Delworth*, 2007]. Among the pressure-based climate indices, the correlation is highest with the AO (Figure 3c); this is confirmed by finding a region over the North American mainland showing persistent strong correlation. For San Francisco (W), the PDO was selected for the SLRM1 model and here we find persistent strong negative correlation with the SST off the coastline of California. For the secondary index, we find relatively week correlation with all pressure-based climate indices. Therefore, we focus on a (persistent) diploe with one COA in the tropical Pacific and another one over the U.S. mainland that does not directly resemble the pattern of one of the known climate indices but may facilitate strong flows toward the site of interest. For Galveston (S), the AMO was selected for the SLRM1 model and we find negative correlation with the SST in the North

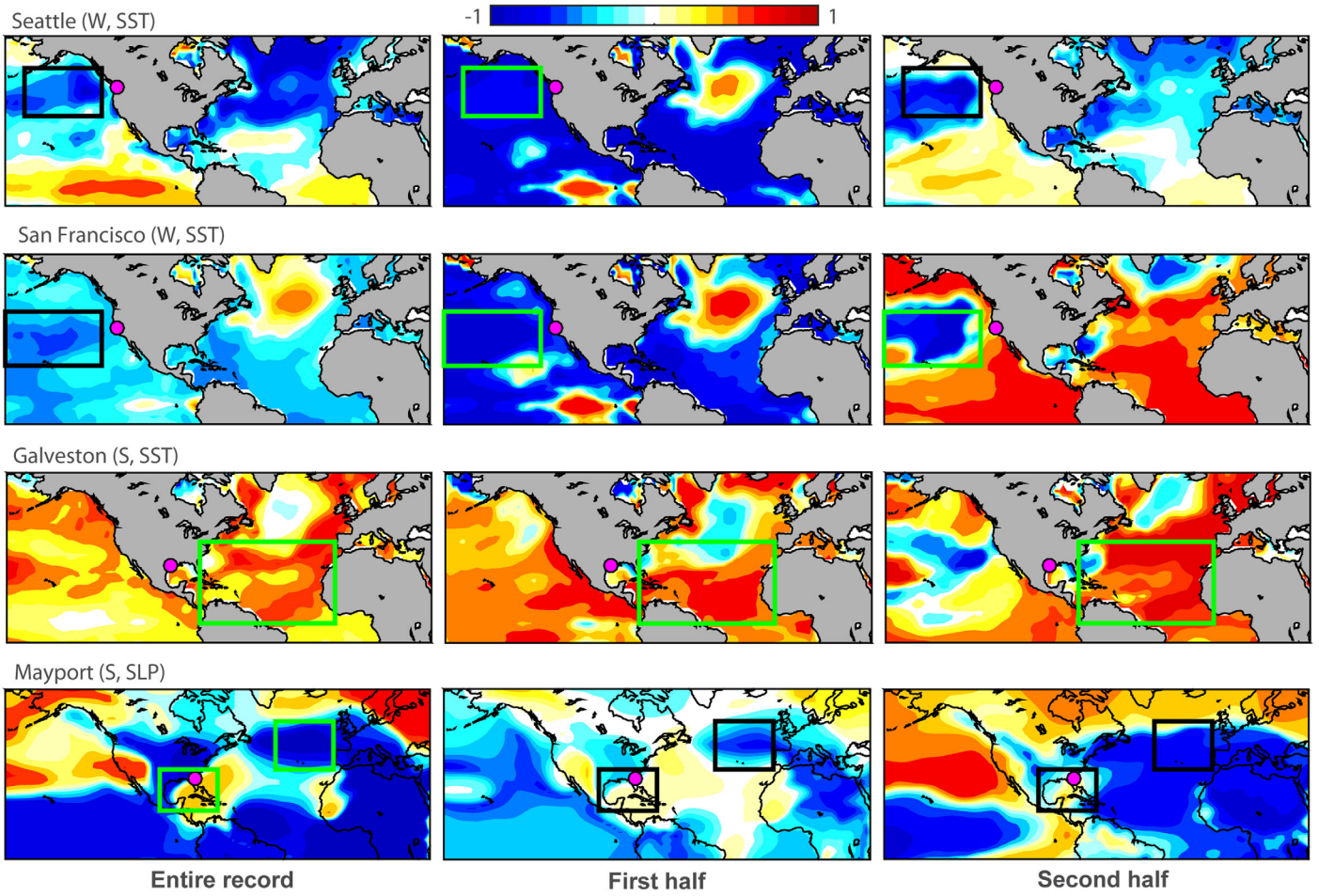

Figure 6. Pointwise correlation between representative RWL time series for the relevant season and low-pass filtered gridded SLP or SST (depending on which index was selected for the SLRM1 models) for the (left) entire record lengths, and the (middle) first and (right) second halves. Regions of interest that we focus on to develop primary tailored indices are highlighted by frames; the magenta-filled circles denote the tide gauge locations.

Atlantic (in the actual AMO region), but much stronger positive correlation further south in the Atlantic and the Caribbean Sea. This is the region where the tropical cyclones typically originate [e.g., *Tannehill*, 1938] that ultimately produce high water levels at the Galveston tide gauge. The secondary index is derived from a NAO-like pattern that we believe affects the hurricane tracks [*Elsner*, 2003]. For Mayport (S), the strongest relationship was found with the NAO and therefore we analyze SLP instead of SST for the primary tailored index. The two COAs are located in the northeast Atlantic and the southeast U.S. and Gulf of Mexico. For the secondary index, we find strong (AMO-like) correlation with SST in the North Atlantic that stretches into the South Atlantic Bight toward the site of interest with an effect on the tropical cyclone activity. The NAO was also selected to predict the winter season RWLs at Mayport, and the location of the COAs is similar (the one in the North Atlantic expands a little bit further westward) but the correlation switches signs. For the secondary index, we focus on a region of strong correlation with the SST in the South Atlantic Bight. For Baltimore (S), the AO was selected in the SLRM1 model and the COAs found from the correlation analysis are again similar to those derived for Mayport (S) (note that the NAO also showed strong correlation with summer RWLs at Baltimore, in addition to the AO). For the secondary index, we find almost the exact same pattern as for Mayport with very strong and AMO-like SST correlation confirming the existence of physical mechanisms linking the AMO and summer RWLs in the southeast of the U.S. Winter RWLs at Atlantic City also showed a strong link to the AMO, and accordingly we find strong correlation with the SST around Iceland and the southern tip of Greenland. The secondary index is constructed from a SLP dipole with one COA over Canada and the other one in the North Atlantic. Finally, for Portland (W), where the NAO was selected in the SLRM1 model, we find one COA in the northwest Atlantic off the U.S. coastline, and the other

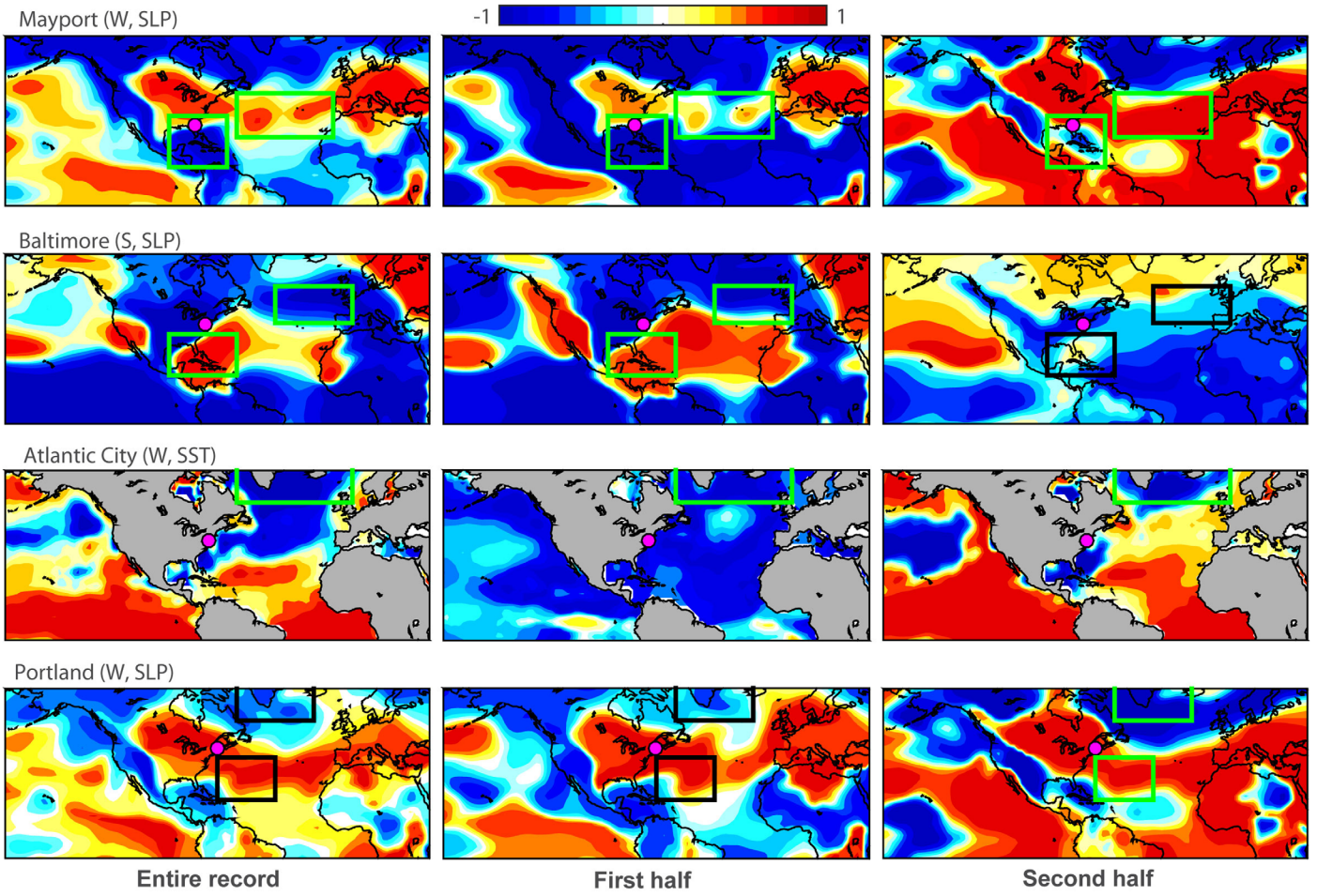

Figure 6. (continued)

one over and around southern Greenland. For the secondary index, we focus on a region of persisting strong negative correlation with SST in the North Atlantic.

The overall spatial patterns in the map extracts shown in Figures 6 and supporting information Figure S2 change substantially when different subsets of the RWL and low-pass filtered SST/SLP time series are used, but within the highlighted regions of interest the correlation remains strong (relative to the surrounding areas) in all cases, especially for the primary indices (Figure 6). The patterns and COA locations also often resemble the ones associated with the climate indices (Figure 5) but the COAs can be refined to allow a more robust and physically meaningful prediction of multidecadal RWL variability.

4.3. Simple and Multiple Linear Regression With Tailored Indices

The SST/SLP grid points exhibiting the strongest correlation (within 5% range of the maxima/minima) with the RWL time series are highlighted in Figure 7. They are used to derive the tailored indices that are subsequently considered as predictors in the SLRM2 and MLRM1 models. To identify potential systematic temporal offsets between changes in RWLs and the large-scale climate, we calculate correlations between the primary tailored indices and the time series representing changes in 100 year RWLs for time lags ranging from -15 to $+15$ years (supporting information Figure S3). In some cases, the correlation gets stronger when time lags of a few years are considered, but these changes are not systematic and negligible (<0.03); hence, we do not account for any time lags when building simple and multiple regression models from the tailored climate indices.

The RWL predictions obtained with the SLRM2 models (Figure 7, left) are similar to those derived with SLRM1, but the explained variance increases at five of the eight sites, now ranging from 49% to 93%, with an average increase of 17%. There are three cases where the explained variances drop (average 11%) when

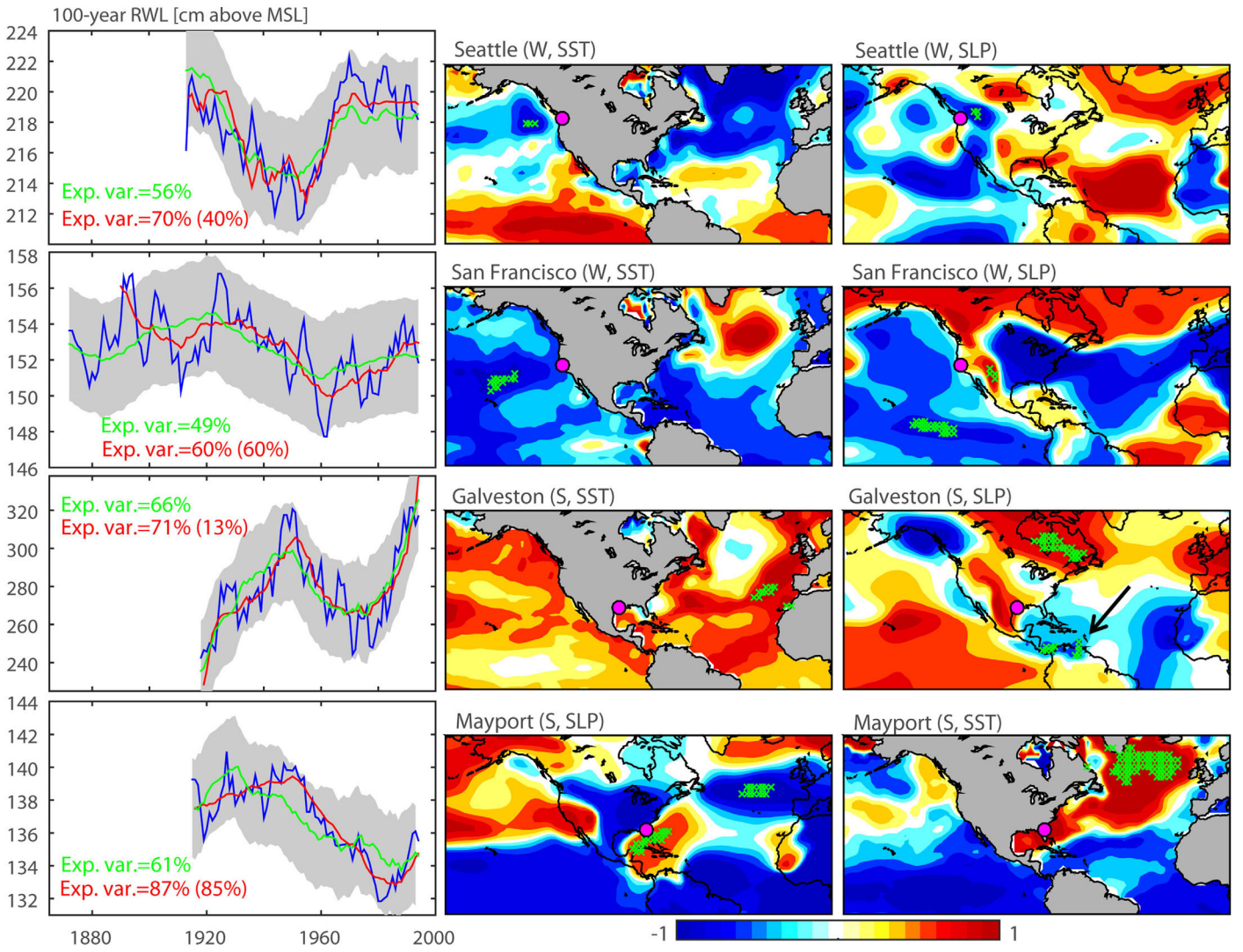

Figure 7. (middle and right) Pointwise correlation between RWL and SST or SLP; grid points with the highest correlation and used for the tailored indices (middle: primary indices; right: secondary indices) are marked by green crosses; tide gauge locations are denoted by the magenta filled circles. (left) RWL changes derived from observations in W15 (blue) and predictions from the SLRM2 (green) and MLRM1 (red) models; numbers in brackets denote the amount of the explained variance when secondary indices are used in simple regression models; gray-shaded bands represent 95% confidence levels of the SLRM2 predictions.

we use the tailored indices instead of the traditional climate indices. For Seattle the AMO showed the strongest correlation but instead of focusing on the region with strong correlation in the North Atlantic, we derived the primary tailored index from SST in the northeast Pacific, where the correlation is a little bit weaker (but still in the order of 0.75, compared to 0.85 around Iceland). In San Francisco, the tailored index goes back to 1854, whereas the PDO starts in 1900. If we build the SLRM2 model from this shorter time period the SLRM1 and SLRM2, predictions become more similar (and the explained variance increases to 53%). The third location where the explained variance drops is Mayport (S). In this case, the NAO was used in the SLRM1 model and we find very strong correlation between the Mayport summer RWLs and SLP over northern Europe and the Norwegian Sea. For the tailored index, however, we focus on the area of high (but a little bit weaker) correlation over the Gulf of Mexico; it is more reasonable to assume a physical connection between the RWLs at Mayport and a SLP dipole with its COAs in the northeast Atlantic and over the Gulf of Mexico (instead of northern Europe/Norwegian Sea).

When we include the secondary indices and use the MLRM1 models for the prediction the explained variance increases to an average of 77% (ranging from 60% to 93% at individual tide gauges). The increase is substantial at some sites (e.g., Mayport (S), Portland (W)) but zero at others, where including the second

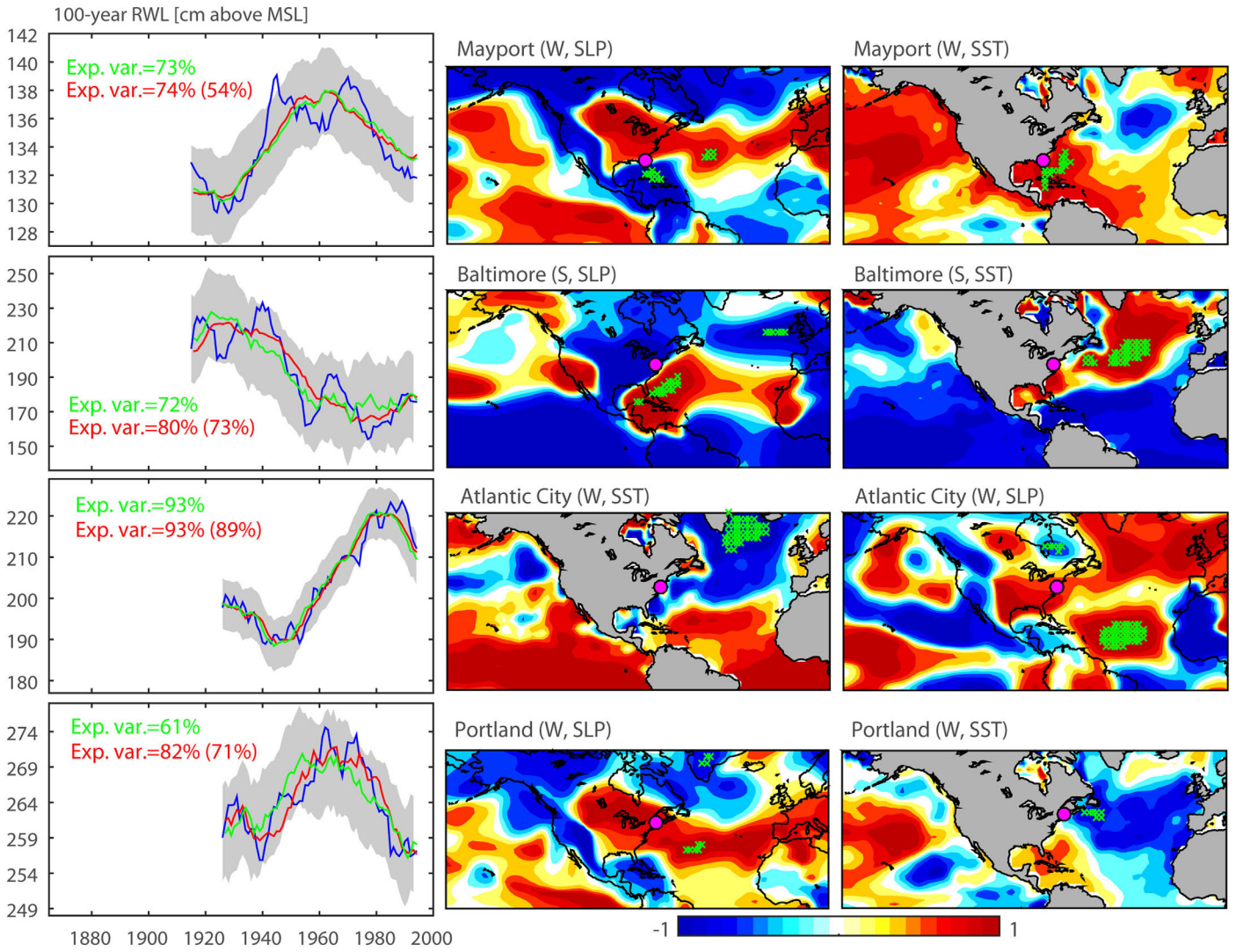

Figure 7. (continued)

predictor does not add any new information to the model. We also test how much variability can be explained by the secondary indices alone when used in a simple regression model (numbers in brackets in Figure 7). At several sites the secondary tailored indices explain as much, or even more, of the variability than the primary indices highlighting the strong coupling between SST and SLP in altering storm surge water levels at multidecadal time scales.

For the last set of models (MLRM2), we include the low-pass filtered wind stress curl time series from the grid points with the strongest correlation in a 10° area around the tide gauge locations as additional predictors. Incorporating wind stress curl into the model leads again to an improvement of the explained variance (Figure 8), now ranging from 60% to 96%; the average increases to 82% (compared to 57% explained with the first set of models SLRM0). With the exception of Mayport (S), the improvement is relatively small or the explained variance with the MLRM2 models is the same as with the MLRM1 models. We also test again how much variability can be explained when using only wind stress curl as predictor (numbers in brackets in Figure 8). The results vary, at some sites it seems to be a poor predictor compared to SST and/or SLP, at others it explains almost as much variability as the other predictors (alone or combined).

We have already tested the spatial stability of the correlation patterns for the tailored indices (Figure 6 and supporting information Figure S2) and have shown that the models—especially SLRM2 and multiple

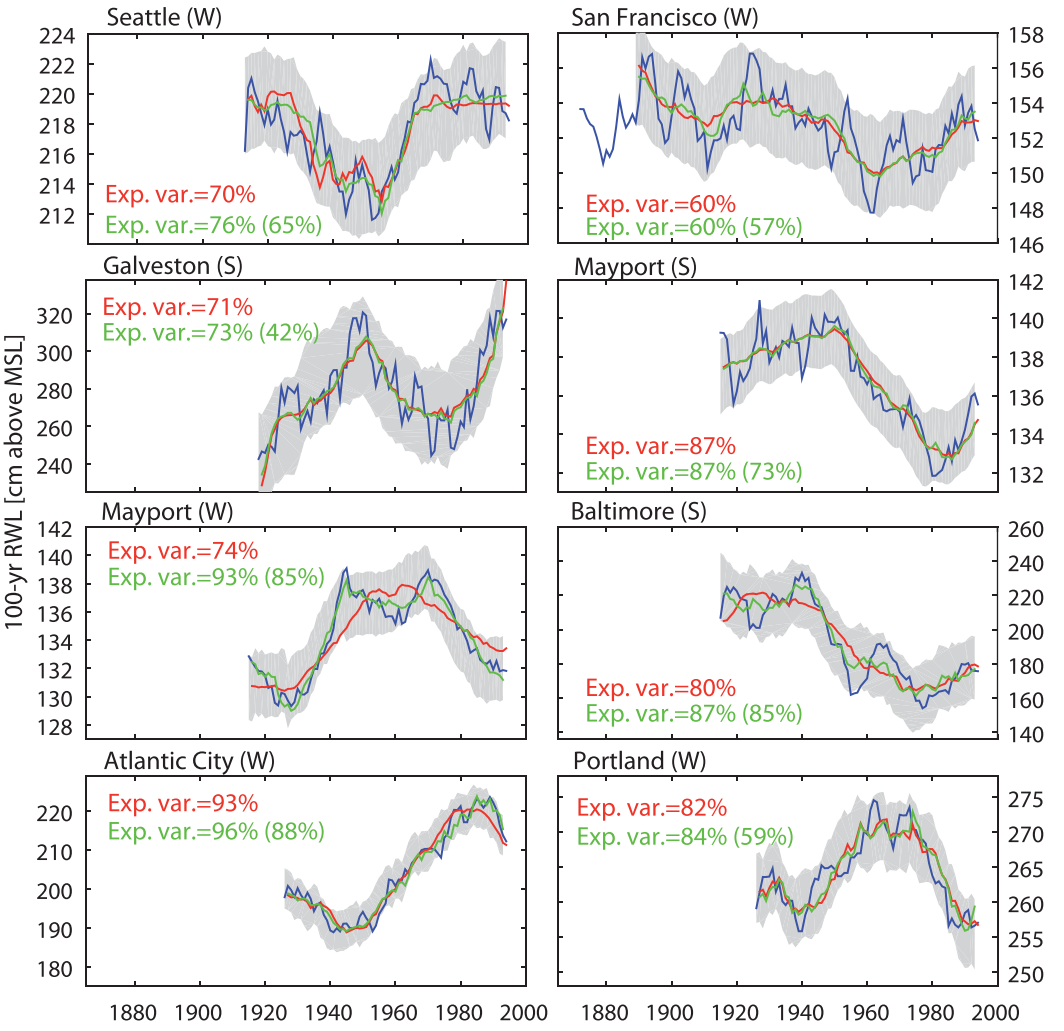

Figure 8. RWL changes derived from observations in W15 (blue) and predictions obtained with the MLRM1 (red) and MLRM2 (green) models; numbers in brackets denote the amount of the explained variance when wind stress curl is used in simple regression models; gray-shaded bands represent 95% confidence levels of the MLRM1 predictions.

regression models MLRM1 and MLRM2—are capable of explaining a large fraction of the multidecadal RWL variability at all sites. Next, in order to test the temporal stability, we fit the models to different data subsets instead of the entire records, and test the stability of the regression coefficients. This is done for the SLRM2 models where we have only one predictor and, exemplarily, for the slope parameter a at San Francisco (W) and Mayport (W) (Figure 9). For San Francisco the regression coefficient becomes stable (i.e., within the range of the 95% confidence bounds derived from fitting the model to the entire data set) for all start years when ~120 years of data are used; for short window lengths (we start with 50 years; i.e., 14 values after applying the nonstationary extreme value analysis/low-pass-filter) the coefficient varies significantly. At Mayport ~80 years of data are enough to derive stable results in relation to the "full model," which is in this case based on shorter records than in San Francisco and therefore the fact that less data are required for stability is not surprising. In both cases, there is a tendency that the coefficients are overestimated when data from the first half are used, while they are underestimated when data from the last few decades are considered. When we increase the window length and use the latter part of the time series in the model, the coefficients become stable earlier (10 years at San Francisco, 3 years at Mayport) than when using the first parts of the data sets. This suggests that the quality of the underlying data sets improves toward the end of the records relative to the 19th century. Similar results and patterns were found for the other sites (not shown).

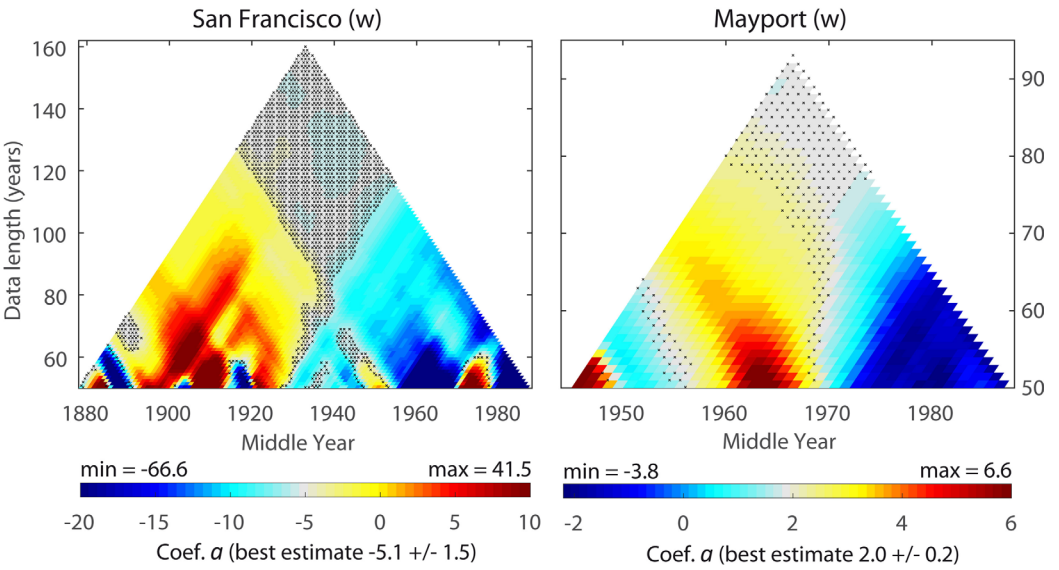

Figure 9. Regression parameter *a* (i.e., the slope parameter) of the SLRM2 models for San Francisco (W) and Mayport (W) for all window lengths and start years; hatched areas denote that the estimated coefficient from the data subset lies within the 95% confidence limits of the best estimate obtained for the full model; color bars were cutoff for presenting purposes, but min/max values are provided.

Finally, we use the predictions that we obtained with the SLRM2, MLRM1, and MLRM2 models as covariates in the extreme value analysis of W15 to test by how much it reduces the range of change in the 100 year RWLs (i.e., the difference between highest and lowest values). In their Figure 10 (black vertical bars), W15 showed that the latter fluctuate by between 9 and 79 cm over time during the relevant seasons at the eight study sites. The results were compared to those derived with a stationary extreme value analysis and exceeded the 95% confidence limits in all cases. The results from the stationary approach are shown as blue-shaded bars in Figure 10 of the present paper (centered on zero); those obtained with the quasi non-stationary extreme value analysis performed in W15 are shown as black vertical bars. When we use the SLRM2 predictions as covariates in the extreme value analysis, the range of change in the 100 year RWLs reduces (Figure 10, green vertical bars) between 12% and 56% (31% on average across all sites) and in most cases proceeds within the uncertainty bands obtained from the stationary assumption. Using the MLRM1 predictions as covariates leads to a reduction of the RWL changes between 17% and 64% (40% on average)

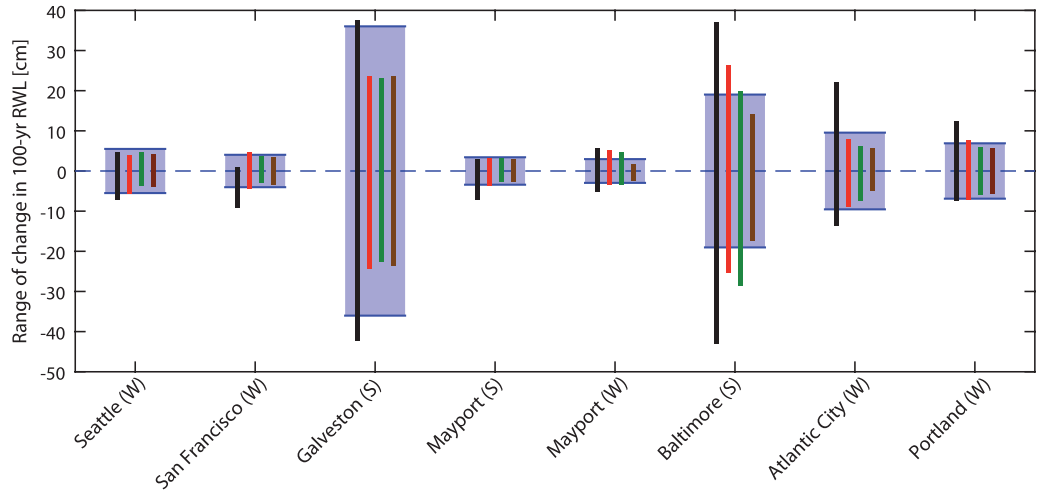

Figure 10. 95% confidence intervals of the 100 year RWLs derived from the stationary extreme value analysis in W15 (blue-shaded bars with horizontal lines); range of change in 100 year RWLs obtained with the quasi nonstationary extreme value analysis performed in W15 (black), and from the same approach but with the SLRM2 (red), MLRM1 (green), and MLRM2 (brown) predictions as covariates; for presenting purposes, the results were vertically adjusted so that the 95% confidence bounds from the stationary analysis are centered on zero.

and using MLRM2 reduces the changes by between 36% and 73% (51% on average). The remaining changes result from the fact that the regression models, although being capable of explaining a large portion of the observed variability, do not capture all the peaks which determine the range of change we are focusing on here.

5. Conclusions

In the present study, we investigated the links between multidecadal variations of design relevant 100 year RWLs (as identified in W15 and summarized in Figure 1) along the U.S. coastline and large-scale climate variability. Multidecadal fluctuations in RWLs—which are currently unaccounted for in design and coastal planning processes—were shown to be considerable (when we follow the procedure that is currently most often used to derive them) and will likely dominate over long-term sea level rise for the next few decades (i.e., coastal management time scales). Therefore, following the long-term objective of being able to project RWL changes into the future, the main focus of the present study was to understand the driving mechanisms of the observed variations and develop statistical models to reconstruct them.

A correlation analysis of the location/scale parameters of the Generalized Extreme Value distribution and the resulting RWLs with various indices, which are known to affect the climate over the U.S. mainland, North Atlantic/Gulf of Mexico, and East Pacific, revealed strong relationships between RWLs and at least one of the climate indices (some of which were also shown to be significantly correlated with each other at multidecadal time scales) (Figure 3). Based on the results from the correlation analysis and "expert judgement" (i.e., when two or more climate indices showed strong correlation with RWLs, we picked the one where a physical connection seems more reasonable) we developed two sets of simple regression models, SLRM0 and SLRM1. Those are able to explain 57% and 59% of the RWL variability, respectively, and also showed that a direct prediction of RWLs leads to similar results than the separate prediction of location and scale parameters and determining the RWLs from them afterwards (Figure 4). Here, we focus on the 100 year RWLs which are most often used for design purposes; the results can, however, be scaled to obtain predictions of the temporal variations for other return levels, e.g., 50 or 1000 years, and if one is interested in the entire distribution the SLRM0 models can be used (along with tailored indices for location/scale parameters from SST, SLP, and wind stress curl if desired).

Since the climate indices used here were originally not defined with the main purpose of predicting multidecadal RWL variations, we developed tailored indices to use them as alternative predictors. They were derived from gridded SLP and SST fields by refining the COAs (after testing their spatial stability) of the traditional climate indices to allow a better and physically more consistent reconstruction of the RWL changes. For each region, we developed primary and secondary indices, one coming from SST the other from SLP; the correlation analysis with the traditional climate indices guided the decision of which variable was used for the primary indices. We then used the primary tailored indices to build the SLRM2 models, which explain on average 66% of the variability (Figure 7). When we use both primary and secondary indices as predictors in a multiple regression model (MLRM1), we can explain 77% of the variability, on average across the region. A last set of models was derived with a multiple linear regression approach where the tailored SST/SLP indices were complemented by a third predictor based on low-pass filtered time series of wind stress curl. With the MLRM2 models, the explained variance increases to 82% on average (Figure 8). Finally, we used the RWL predictions as covariates in the nonstationary extreme value analysis and tested how much of the range of change in 100 year RWLs can be explained. The MLRM1 and MLRM2 (and in most cases also the SLRM2) models allow to turn a nonstationary process into a stationary one at all sites (Figure 10), thereby cutting the range of change almost into half.

This implies that one would be able—given that climate models are capable of simulating temporal changes in the variables used here as predictors (SLP, SST, and wind)—to project a major fraction of the nonstationarity (or temporal changes) in design relevant RWLs into the future, and to include the information into decision making in the climate adaptation context. Using computationally efficient statistical models for this purpose allows one to include all representative concentration pathways and to evaluate individual climate models (thereby accounting for the full range of scenario and model uncertainties) as well as ensembles comprising all models, or only those that are able to reconstruct much of the observed RWL variability. This will be explored in a future investigation.

Acknowledgments

T.W. was supported by a fellowship within the postdoctoral program of the German Academic Exchange Service (DAAD). D.P.C was supported under a grant from the NASA Interdisciplinary Science Sponsored Research program. The tide gauge data used in W15 to obtain the RWL time series used here are freely accessible through the University of Hawaii Sea Level Center database (uhslc.soest.hawaii.edu/data/) and NOAA's Tides and Currents website (http://tidesandcurrents.noaa.gov/). Climate indices were derived from the website of the Global Climate Observing System (GCOS) Working Group on Surface Pressure (WG-SP) (http://www.esrl.noaa.gov/psd/gcos); the station-based NAO was downloaded from NCAR/UCAR's Climate Data Guide website: https://climatedataguide.ucar.edu/. Sea surface temperature (ERSST v3b), as well as sea level pressure, and wind data from the 20th Century Reanalysis Project were downloaded from NOAA's Physical Sciences Division website: http://www.esrl.noaa.gov/psd/. We are grateful to Francisco M. Calafat for calculating and providing the wind stress curl data.

References

Bernhardt, J. E,. and A. T. DeGaetano (2012), Meteorological factors affecting the speed of movement and related impacts of extratropical cyclones along the U.S. east coast, *Nat Hazards*, *61*, 1463–1472.

Bromirski, P. D., R. E. Flick, and D. R. Cayan (2003), Storminess variability along the California coast: 1858–2000, *J. Clim.*, *16*, 982–993, doi: 10.1175/1520-0442(2003)016<0982:SVATCC>2.0.CO;2.

Cayan, D. R., P. D. Bromirski, K. Hayhoe, M. Tyree, M. Dettinger, and R. E. Flick (2008), Climate change projections of sea level extremes along the California coast, *Clim. Change*, *87*, 57–73, doi:10.1007/s10584-007-9376-7.

Church, J. A., et al. (2013), Sea level change, in *Climate Change 2013: The Physical Science Basis. Contribution of Working Group I to the Fifth Assessment Report of the Intergovernmental Panel on Climate Change*, edited by T. F. Stocker, et al., pp. 1137–1216, Cambridge Univ. Press, Cambridge, U. K.

Compo, G. B., et al. (2011), The twentieth century reanalysis project, *Q. J. R. Meteorol. Soc.*, *137*, 1–28, doi:10.1002/qj.776.

Dangendorf, S., S. Müller-Navarra, J. Jensen, F. Schenk, T. Wahl, and R. Weisse (2014), North Sea Storminess from a Novel Storm Surge Record since AD 1843, *J. Clim.*, *27*, 3582–3595, doi:10.1175/JCLI-D-13-00427.1.

Elsner, J. B. (2003), Tracking hurricanes, *Bull. Am. Meteorol. Soc.*, *84*(3), 353–356.

Enfield, D. B., A. M. Mestas-Nunez, and P. J. Trimble (2001), The Atlantic Multidecadal Oscillation and its relationship to rainfall and river flows in the continental U.S., *Geophys. Res. Lett.*, *28*, 2077–2080.

Grinsted, A., J. C. Moore, and S. Jevrejeva (2013), Projected Atlantic hurricane surge threat from rising temperatures, *Proc. Natl. Acad. Sci. U. S. A.*, *110*, 5369–5373, doi:10.1073/pnas.1209980110.

Hurrell, J.W. (1995), Decadal trends in the North Atlantic oscillation: Regional temperatures and precipitation, *Science*, *269*, 676–679.

Jaccard, J., R. Turrisi, and C. K. Wan (1990), Interaction effects in multiple regression, in *Quantitative Applications in the Social Sciences, Sage Univ. Pap. Ser., 07-069*, Sage Newbury Park, Calif.

Kennedy, A. J., M. L. Griffin, S. L. Morey, S. R. Smith, and J. J. O'Brien (2007), Effects of El Niño–Southern Oscillation on sea level anomalies along the Gulf of Mexico coast, *J. Geophys. Res.*, *112*, C05047, doi:10.1029/2006JC003904.

Komar, P. D., J. C. Allan, and P. Ruggiero (2011), Sea level variations along the US Pacific Northwest coast: Tectonic and climate controls, *J. Coastal Res.*, *27*(5), 808–823.

Mantua, N. J., S. R. Hare, Y. Zhang, J. M. Wallace, and R. C. Francis (1997), A Pacific decadal climate oscillation with impacts on salmon production, *Bull. Amer. Meteorol. Soc.*, *78*, 1069–1079.

Marcos, M., F. M. Calafat, Á. Berihuete, and S. Dangendorf (2015), Long-term variations in global sea level extremes, *J. Geophys. Res. Oceans*, *120*, doi:10.1002/2015JC011173.

Méndez, F. J., M. Menéndez, A. Luceño, and I. J. Losada (2007), Analyzing monthly extreme sea levels with a time-dependent GEV model, *J. Atmos. Oceanic Technol.*, *24*(5), 894–911.

Park J., J. Obeysekera, M. Irizarry-Ortiz, J. Barnes, and W. Park-Said (2010a), Climate links and variability of extreme sea level events at Key West, Pensacola, and Mayport Florida, *J Waterrw. Port Coastal Ocean Eng.*, *136*, 350–356, doi:10.1061/(ASCE)WW.1943-5460.0000052.

Park J., J. Obeysekera, and J. Barnes (2010b), Temporal energy partitions of Florida extreme sea level events as a function of Atlantic multidecadal oscillation, *Ocean Sci.*, *6*, 587–593.

Rayner N. A., D. E. Parker, E. B. Horton, C. K. Folland, L. V. Alexander, D. P. Rowell, E. C. Kent, and A. Kaplan (2003), Global analyses of sea surface temperature, sea ice, and night marine air temperature since the late nineteenth century, *J. Geophys. Res.*, *108*(D14), 4407, doi: 10.1029/2002JD002670.

Ropelewski, C. F., and P. D. Jones (1987), An extension of the Tahiti-Darwin southern oscillation index, *Mon. Weather Rev.*, *115115*, 2161–2165.

Serafin, K. A., and P. Ruggiero (2014*)*, Simulating extreme total water levels using a time-dependent, extreme value approach, *J. Geophys. Res. Oceans*, *119*, 6305–6329, doi:10.1002/2014JC010093.

Sweet, W. V., and C. Zervas (2011), Cool-season sea level anomalies and storm surges along the U.S. East Coast: Climatology and comparison with the 2009/10 El Niño, *Mon. Weather Rev.*, *139*, 2290–2299.

Talke, S. A., P. Orton, and D. A. Jay (2014), Increasing storm tides in New York Harbor, 1844–2013, *Geophys. Res. Lett.*, *41*, 3149–3155, doi: 10.1002/2014GL059574.

Tannehill, I. R. (1938), *Hurricanes*, 257 pp., Princeton Univ. Press, Princeton, N. J.

Thompson, D. W. J., and J. M. Wallace (1998), The Arctic oscillation signature in the wintertime geopotential height and temperature fields, *Geophys. Res. Lett.*, *25*, 1297–1300.

Thompson, P. R., G. T. Mitchum, C. Vonesch, and J. Li (2013), Variability of winter storminess in the eastern United States during the twentieth century from tide gauges, *J. Clim.*, *26*, 9713–9726.

Trenberth, K. E., and J. W. Hurrell (1994), Decadal atmosphere-ocean variations in the Pacific, *Clim. Dyn.*, *9*, 303–319.

Wahl, T., *and* D. P. Chambers (2015), Evidence for multidecadal variability in US extreme sea level records, *J. Geophys. Res. Oceans*, *120*, 1527–1544, doi:10.1002/2014JC010443.

Zhang, R., and T. L. Delworth (2007), Impact of the Atlantic multidecadal oscillation on North Pacific climate variability, *Geophys. Res. Lett.*, *34*, L23708, doi:10.1029/2007GL031601.